IOP Publishing Measurement Science and Technology
Meas. Sci. Technol. **31** (2020) 044002 (12pp) https://doi.org/10.1088/1361-6501/ab4cc7

A hidden corrosion detection method based on robust multimodal Lamb waves

Zhi Luo[1], **Liang Zeng**[1] and **Jing Lin**[1,2,3]

[1] State Key Laboratory for Manufacturing Systems Engineering, School of Mechanical Engineering, Xi'an Jiaotong University, Xi'an, Shaanxi Province 710049, People's Republic of China
[2] School of Reliability and Systems Engineering, Beihang University, Haidian District, Beijing 100191, People's Republic of China

E-mail: linjing@buaa.edu.cn

Received 30 June 2019, revised 8 October 2019
Accepted for publication 10 October 2019
Published 8 January 2020

Abstract

A Lamb wave is a kind of elastic wave propagating in a plate-like structure with stress distributing through the whole thickness of the plate. A Lamb wave is multimodal, and each mode has unique through-plate-thickness stress profiles, called wave structure. The existence of a specific structure flaw at a certain position in the thickness direction will weaken the ability of the plate to support a specific component of stress, which means each Lamb wave mode would interact with structure flaws in a different way, or that each Lamb wave mode has a unique sensitivity to flaws. Conventionally, a sensitive single mode has been selected for defect detection. However, due to the inconsistency in actuators or sensors, the robustness of detection is limited. In this paper, the difference in the sensitivity of each mode to flaws, rather than a single mode, was used for defect detection. Based on this idea, numerical and experimental studies of the interaction between hidden corrosion and multiple modes were first conducted. Then, a new index, the relative amplitude coefficient, which evaluates the difference in sensitivity between lowest-order modes and higher-order modes, was proposed. Next, by using a double crosshole array and combining it with a probabilistic reconstruction algorithm, a multimodal Lamb wave corrosion detection method was developed. The results show greater robustness in corrosion location and better accuracy, compared with the location results of conventional single mode defect detection. Furthermore, by applying the double sensor strategy, the effective operating frequency range is extended and the location accuracy enhanced.

Keywords: multimodal Lamb wave, two-dimension Fourier transform, frequency-wavenumber domain distribution, interaction with defect, corrosion detection

(Some figures may appear in colour only in the online journal)

1. Introduction

Hidden corrosion is a kind of threatening thin wall structure flaw and its detection is a serious problem. Conventional ultrasonic bulk waves are usually limited by the poor time resolution in thin wall structures due to a series of unclear echoes [1]. With great sensitivity to abnormalities near the propagation path, Lamb waves are considered a promising nondestructive evaluation method for plate-like structures [2–6]. Lamb wave propagation properties in plates are dependent on the thickness and material properties of the structure. Structural flaws would affect the propagation properties of multimodal Lamb waves [7]. Therefore, before developing a Lamb-wave-based hidden corrosion detection method, the interaction between structure flaws and the individual Lamb wave mode needs to be studied.

Kundu *et al* [8] proposed the idea that the existence of a specific structure flaw at a certain position in the thickness direction will weaken the ability of the plate to support a specific component of stress. Alleyne and Cawley [3, 9] proposed

[3] Author to whom any correspondence should be addressed.

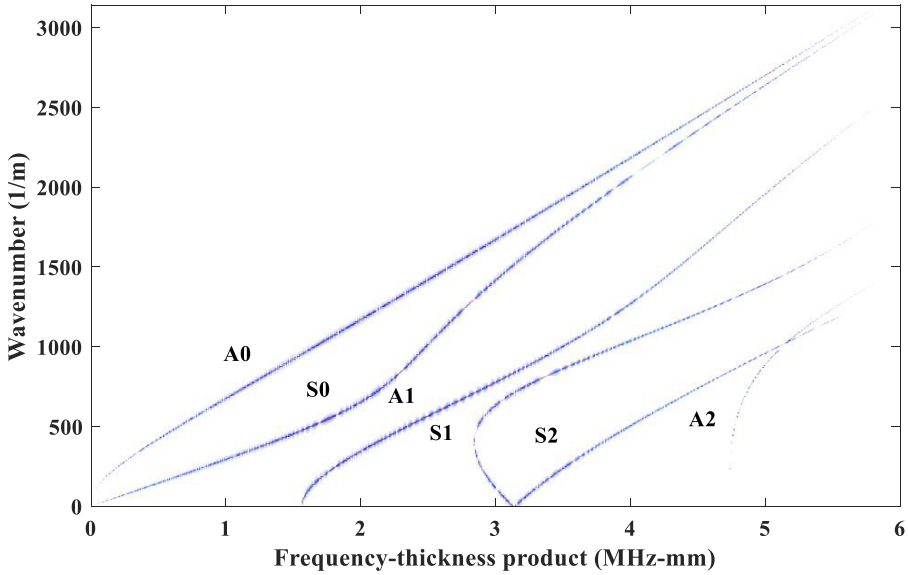

Figure 1. Frequency-wavenumber domain distribution of simulated 4000 equal space step recorded signals.

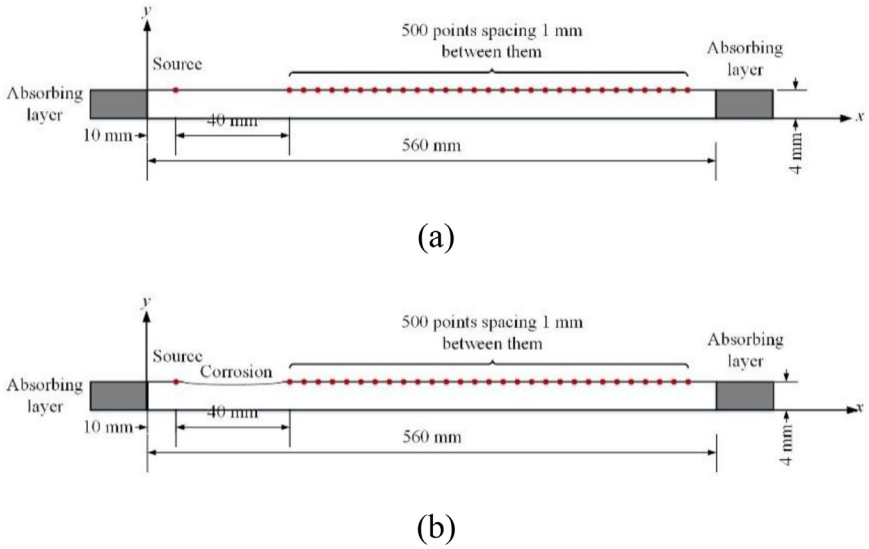

Figure 2. Configuration of numerical modeling. (a) Normal aluminum plate. (b) Corroded aluminum plate.

a 2D Fourier transform method and quantified the interactions between multiple modes and structure flaws in both experimental and finite element numerical investigations. Zhu and Rose [1] presented a quantitative technique for hidden corrosion depth based on the numerical studies by a hybrid boundary element method. Lee and Staszewski [10] proposed the local interaction simulation approach (LISA) for Lamb wave propagation modelling and studied 2D wave interactions with notches. Leonard *et al* [11] developed a Lamb wave tomographic reconstruction method based on the frequency-dependent velocity of the dispersive Lamb wave mode. Zhao *et al* [12] developed a Vold–Kalman filter in the time–frequency domain to extract interfered wave modes and estimated quantitative propagation characteristics of waveforms from damage. Besides, some researchers had investigated scattering and mode conversion of Lamb waves from various defects [13–16].

According to the previous studies, multimodal Lamb modes show different sensitivities to different specific defect types. Some corrosion detection methods were developed. Zhu *et al* [17] studied several feature variations, such as mode cutoff, group velocity changes, mode frequency shifts, and transmission and reflection amplitudes. Silva *et al* [18] showed that the loss of the S1 mode near its cutoff frequency can be used for corrosion detection. Zeng *et al* [19] applied the nondispersive S0 mode for propagation distance correction, which helped Lamb wave tomography in corrosion detection.

In this paper, the numerical modeling and experimental study was first conducted to investigate the interaction between the structure flaws and multiple Lamb wave modes.

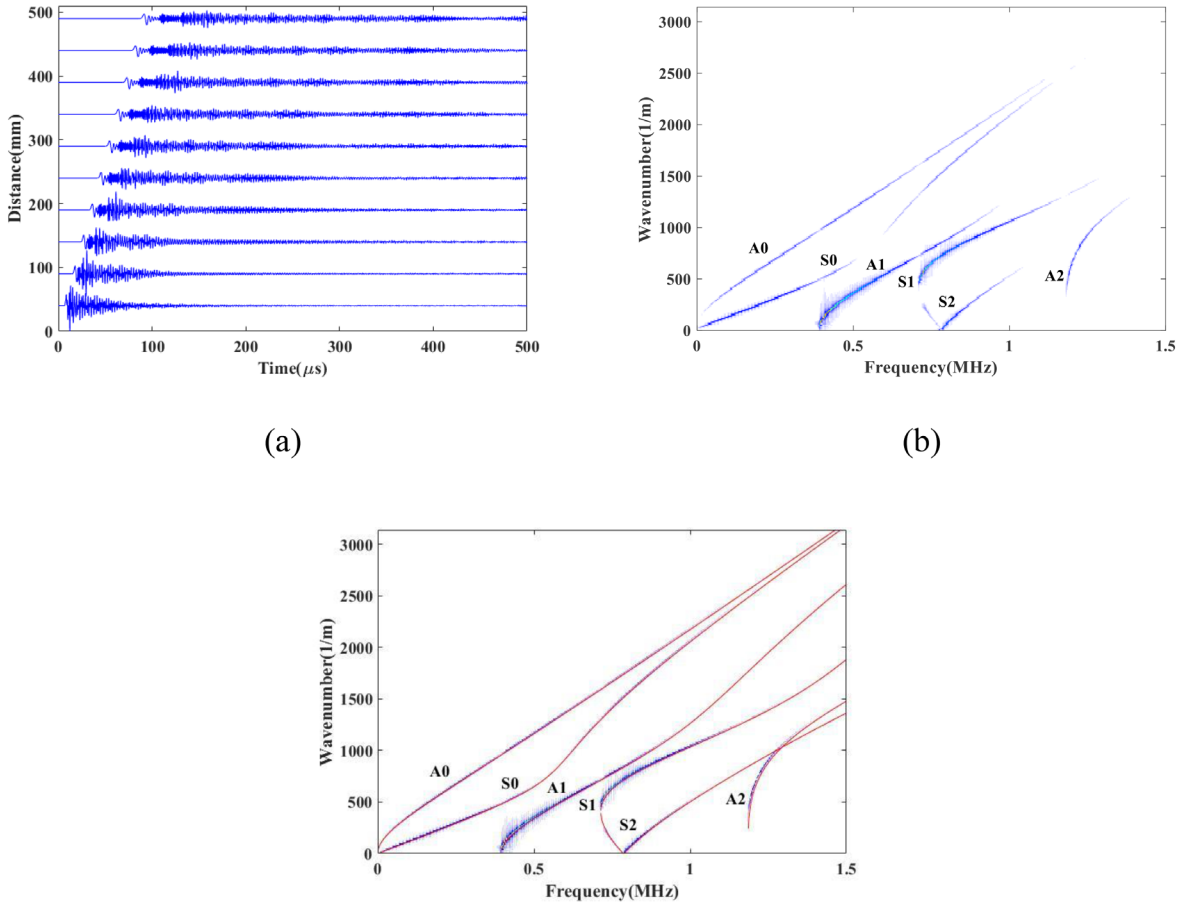

Figure 3. Numerical results of the normal plate. (a) Time histories of the response of the top surface of the normal plate. (b) The frequency-wavenumber domain distribution of the 500 equal space step recorded signals. (c) Comparison between the numerical frequency-wavenumber domain distribution and theoretical dispersion curves.

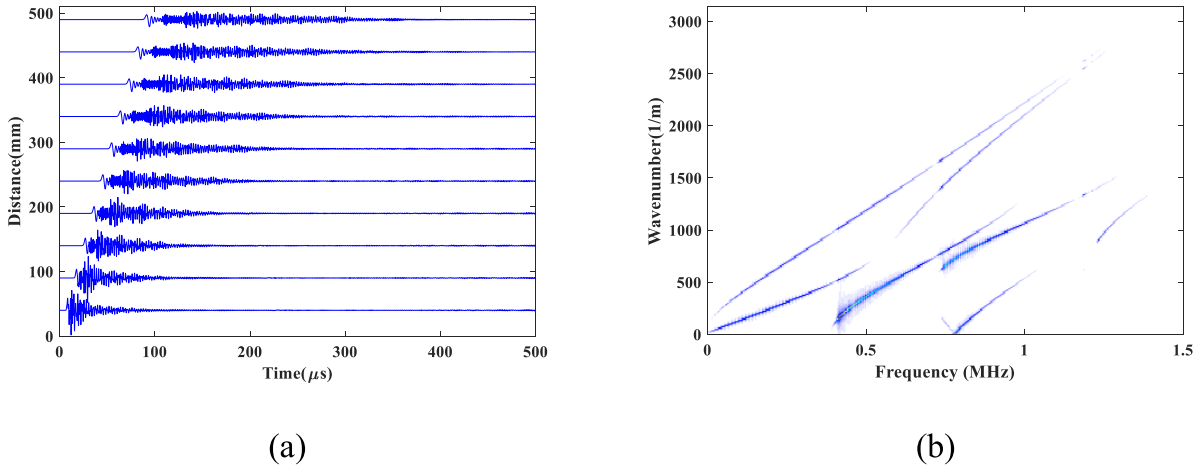

Figure 4. Numerical results of the corroded plate. (a) Time histories of the response of the top surface of the normal plate. (b) The frequency-wavenumber domain distribution of the 500 equal space step recorded signals.

Based on the numerical and experimental results, a new index exploiting the multimodal Lamb wave feature, which is robust regardless of inconsistency in sensors, was proposed. Then, combined with a probabilistic reconstruction algorithm, a corrosion detection method was developed.

2. Method

Assuming a Lamb wave propagating in a free plate, the displacement on the surface, denoted by $u(x, t)$, can be represented:

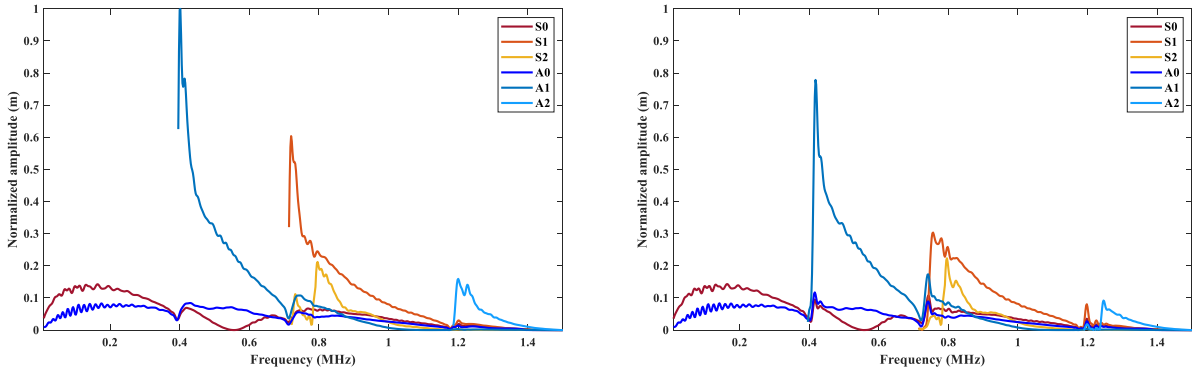

Figure 5. Amplitude distribution curve of each mode. (a) The normal plate. (b) The corroded plate.

$$u(x,t) = A(\omega)\int_{-\infty}^{\infty} F(\omega)\mathrm{e}^{-\mathrm{i}k(\omega)x}\mathrm{e}^{\mathrm{i}\omega t}\mathrm{d}\omega \tag{1}$$

where $A(\omega)$ is the response amplitude of the Lamb wave mode, $k(\omega)$ is the wavenumber of the Lamb wave mode, and $F(\omega)$ is the Fourier transformation of the excitation $f(t)$.

Propagating Lamb waves are sinusoidal in both the frequency and wavenumber domains. Therefore, a time domain signal can be transformed to the frequency domain by a temporal Fourier transform, and a space domain signal can be mapped to the wavenumber domain by a spatial Fourier transform. With a series of time-space domain signals carried out by a 2D Fourier transform, the amplitudes and wavenumbers of individual modes would be cleared in a frequency-wavenumber domain [3].

$$H(k,f) = \int_{-\infty}^{\infty}\int_{-\infty}^{\infty} u(x,t)\mathrm{e}^{-\mathrm{i}(kx+\omega t)}\mathrm{d}x\mathrm{d}t. \tag{2}$$

Figure 1 shows a 2D Fourier transform of 4000 simulated Lamb wave signals. The simulation was conducted according to equation (1). The excitation $f(t)$ is a one-cycle Hanning windowed sine signal centered at 500 kHz. The response amplitude $A(\omega)$ was set as one for each mode. The sampling frequency is 20 MHz and the space interval of 4000 recorded points is 1 mm.

As shown in figure 1, A0, S0, A1, S1, S2 and A2 modes are discerned clearly in a frequency-wavenumber domain. Compared with the theoretical dispersion curves, the frequency-wavenumber distribution is highly matched.

3. Numerical modeling

3.1. Numerical setup

Commercial finite element (FE) software, Comsol, had been used for 2D simulation of Lamb wave propagation. The numerical modeling was carried out in a solid mechanic module, transient study (or time-dependent study). The aluminum plate ($\rho = 2700\,\mathrm{kg\ m^{-3}}$, $E = 7.17\times10^{10}$ Pa, $\mu = 0.33$) is 4 mm thick and 560 mm long. Two absorbing layers were arranged at both ends of the plate to avoid boundary reflections, as shown in figure 2(a). *X*-direction displacement was loaded at the source with a one-cycle Hanning windowed sine signal centered at 500 kHz. The distance between the generating point and the first received point is 40 mm. 500 points acted as the received sensors to record the *x*-direction displacement signal with a 1 mm space interval between each one.

The element size should be less than one-tenth of a wavelength, 0.15 mm in the model. Based on the CFL condition and Nyquist criteria, the time step was set as 25 ns. In order to figure out how Lamb wave modes interact with defects, a 0.2 mm deep and 35 mm diameter oval corrosion was set between the source and the first receive point, as shown in figure 2(b).

3.2. Numerical results

Figure 3(a) shows some time histories of the response of the top surface of a normal plate. By applying a 2D Fourier transform to the 500 time histories, the frequency–wavenumber domain distribution of the Lamb wave in the normal aluminum plate was obtained, as shown in figure 3(b). The frequency–wavenumber relationship matched the theoretical dispersion curves well, as shown in figure 3(c). Figures 4(a) and (b) show the recorded signals and the frequency–wavenumber domain distribution of Lamb waves in a corroded plate, respectively. Comparing figure 4(b) with 3(b), there seems to be no difference in the frequency–wavenumber relationship but a slight difference in amplitude, especially near the cutoff frequencies of all higher-order modes in these two plates. The amplitude difference shows that the corrosion greatly affects the transmission coefficient of higher-order modes.

In the frequency–wavenumber domain distribution, due to the sparse nature, every individual mode can be extracted and the amplitude distribution can be calculated by integrating the amplitude in a small region near the dispersion curves. Figures 5(a) and (b) show the amplitude distribution of the normal plate and corroded plate. It should be noted that there is no significant difference between the normal plate and the corroded plate in the response amplitude of the lowest-order modes, A0 and S0, under the first cutoff frequency. Namely, the lowest-order modes are insensitive to the corrosion. The

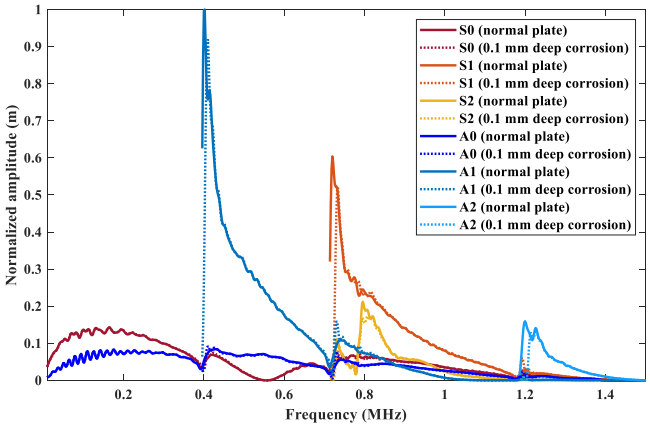

(a)

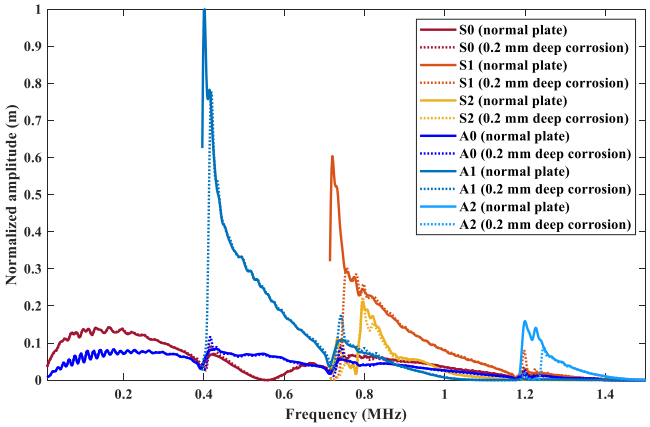

(b)

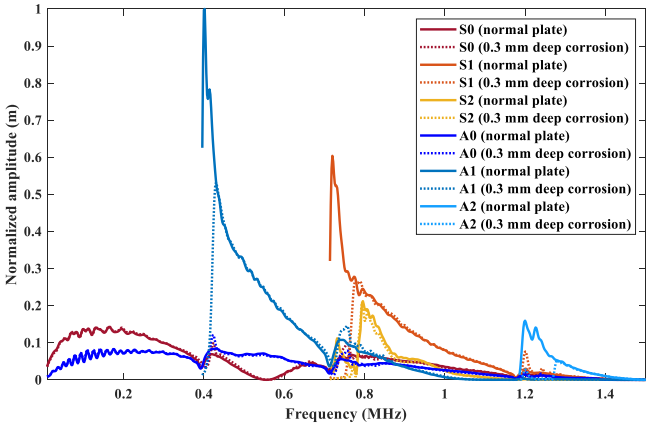

(c)

Figure 6. Amplitude distribution curves of three aluminum plates with different ellipsoidal corrosions, with the same 35 mm diameter but different depths. (a) 0.1 mm deep. (b) 0.2 mm deep. (c) 0.3 mm deep.

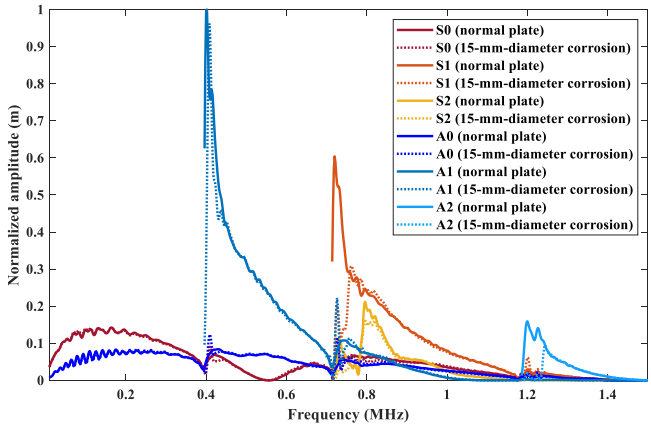

(a)

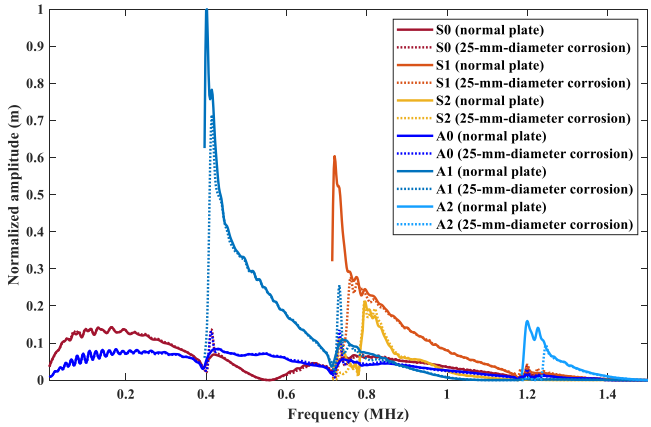

(b)

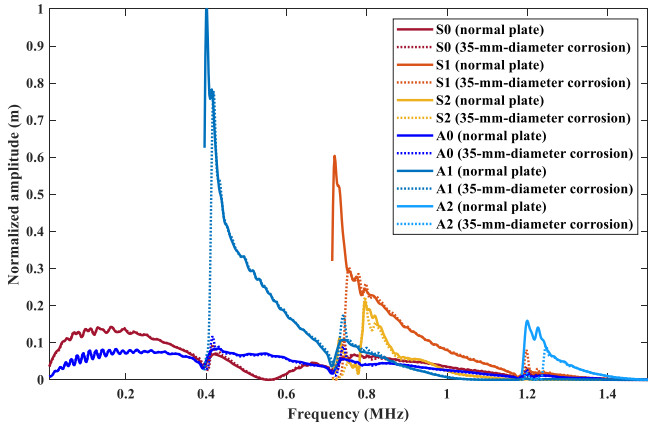

(c)

Figure 7. Amplitude distribution curves of three aluminum plates with different ellipsoidal corrosions, with the same 0.2 mm depth but different diameters. (a) 15 mm diameter. (b) 25 mm diameter. (c) 35 mm diameter.

situation is different for higher-order modes. Almost all the higher-order modes have a peak value near their cutoff frequencies in the normal plate. While, after introducing the corrosion, these peak values decreased. With the frequency increasing away from the cutoff frequency, these higher-order modes turn insensitive to the corrosion. The main reason may be, according to the wave structure, that each higher-order mode gets the largest in-plane displacement at its cutoff frequency, and with increasing frequency, the proportion of in-plane displacement decreases [2]. In a word, the closer the operating frequency is to the cutoff frequency, the more sensitive a higher-order mode is to defects.

In these amplitude distribution curves, another interesting phenomenon that should be noted is that at the cutoff

frequencies of all higher-order modes, mode conversion occurs. For example, A0 and S0 modes show an amplitude increase at A1 mode cutoff frequency, and A0, S0 and A1 mode increase at S1 mode cutoff frequency. The energy transmitted through the defect and converted to lower order modes may explain the amplitude loss of higher-order modes.

3.3. Parametric studies

In order to investigate how the hidden corrosion influences the transmitted signals, a series of numerical models were also built and the transmission characteristics through corrosions were studied.

Figure 6 shows the amplitude distribution curves of three aluminum plates with different ellipsoidal corrosions, with the same 35 mm diameter but different depth (0.1 mm, 0.2 mm, 0.3 mm). In order to reveal how higher-order mode interacts with the corrosions, the amplitude distribution curves of the normal plate were also shown in figures 6(a)–(c) for comparison.

As can be seen, except for near the cutoff frequency of each higher-order mode, the amplitude distribution curves remain almost the same in most frequency ranges, regardless of the depth of corrosions. However, in the frequency range near the cutoff frequency of each higher-order mode, with an increase in the depth of corrosions, the difference between the normal plate and the corroded plate enlarges. Due to the introduction of corrosions and the occurrence of mode conversion, amplitude curves of each higher-order mode near the cutoff frequency are transferred to other lower-order modes, which can be regarded as a shift of cutoff frequency. With the depth of corrosion increased from 0.1 mm to 0.3 mm, the frequency gaps of peak value of each higher-order mode between corroded plates and the normal plate are 8 kHz, 16 kHz and 28 kHz (A1 mode); 14 kHz, 36 kHz and 58 kHz (S1 mode); and 14 kHz, 46 kHz and 80 kHz (A2 mode). As can be seen, the higher the mode is, the larger the frequency gap is, which refers to better sensitivity. Comparing with the cutoff frequencies of each higher-order mode (396 kHz for A1 mode, 714 kHz for S1 mode, and 1186 kHz for A2 mode), the relative shift of cutoff frequency is about 2% for a 0.1 mm-deep corroded plate; about 4% for a 0.2 mm-deep corroded plate; and about 7% for a 0.3 mm-deep corroded plate. These percentages are close to the relative thickness loss (2.5% for a 0.1 mm-deep corrosion; 5% for a 0.2 mm-deep corrosion; 7.5% for a 0.3 mm-deep corrosion). Therefore, the shift in cutoff frequency may be a promising index referring to thickness loss in structure.

After the influence of the depth of corrosions in the transmission coefficient characteristics studied, some corrosions with the same depth but different diameters (15 mm, 25 mm and 35 mm) were also introduced into the numerical studies. The results are shown in figure 7. With the diameter of the corrosion increased from 15 mm to 35 mm, the frequency gaps are 6 kHz, 40 kHz and 44 kHz (A1 mode), 12 kHz, 40 kHz and 46 kHz (S1 mode), and 16 kHz, 36 kHz and 46 kHz (S2 mode). Except for A1 mode, the shift of the cutoff frequency of other higher-order modes remains almost the same, which means that the law of mode conversion in corroded plates was almost the same regardless of the diameter of corrosions. According to numerical studies in models with different sized corrosions, this conclusion is only tenable when the diameter of the corrosion is large enough. In the numerical models, the diameter should be greater than 10 mm.

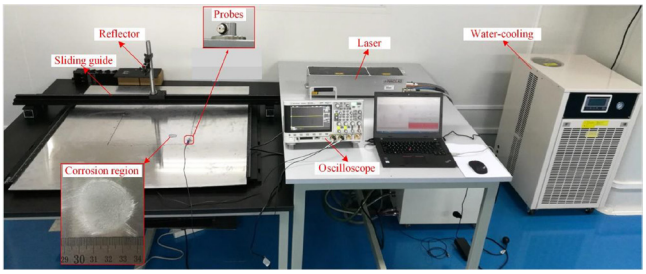

Figure 8. Experimental setup.

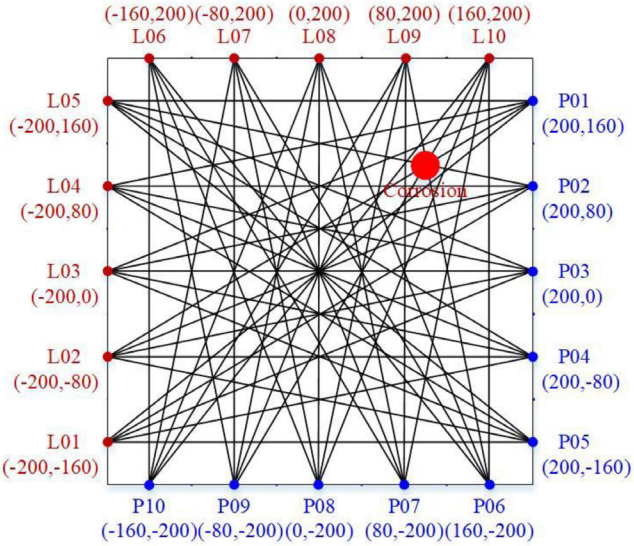

Figure 9. Measurement arrangement (unit: mm).

4. Experimental investigation

4.1. Experimental setup

The experiment was conducted on an aluminum plate (1 m × 1 m × 3.9 mm, seen in figure 8). An Innolas Spitlight 600-10 YAG laser acted as the actuator for Lamb wave generation due to the thermoelastic effect (wavelength: 1064 nm, unfocused beam diameter: 6 mm). An Olympus C133-RM ultrasonic probe (center frequency: 2.25 MHz, element size: 6 mm) acted as the receiver for wideband Lamb wave recording. An Agilent DSOX-3014A oscilloscope recorded the signals from the ultrasonic probe with a 20 MHz sampling frequency. The time duration of the recorded signals is 0.5 ms. The laser hit point moved through the aluminum plate by sliding an optical reflector on a guided rail. The received point scanned by moving the probes manually. A simulated corrosion was ground by sandpaper on the top surface. The ellipsoidal corrosion is 35 mm in diameter and the largest depth is 0.2 mm.

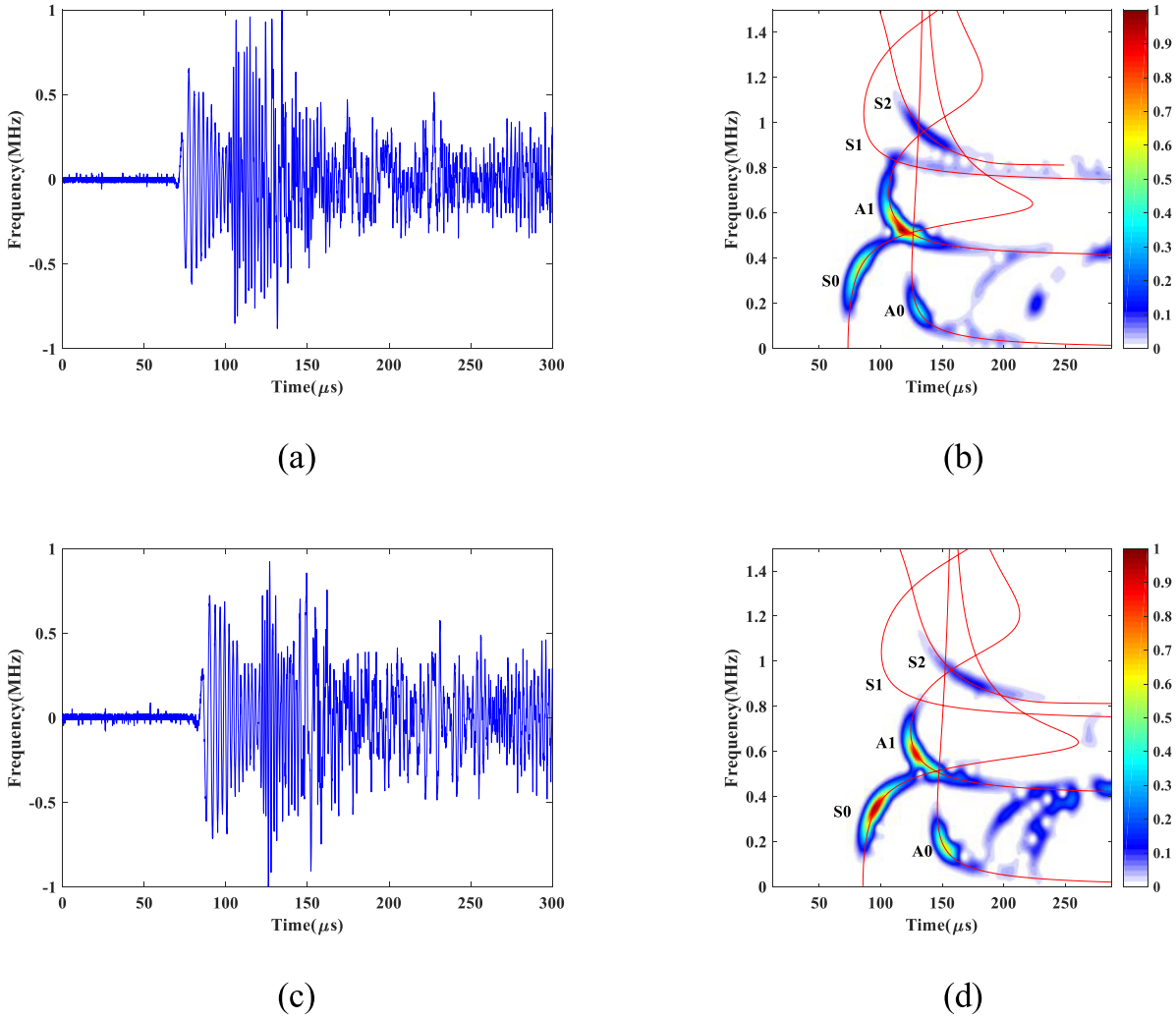

Figure 10. (a) Time domain signals recorded from the normal path L02-P04. (b) Normalized time–frequency spectrum of signal from L02-P04. (c) Time domain signals recorded from the corroded path L02-P01. (b) Normalized time–frequency spectrum of signal from L02-P01.

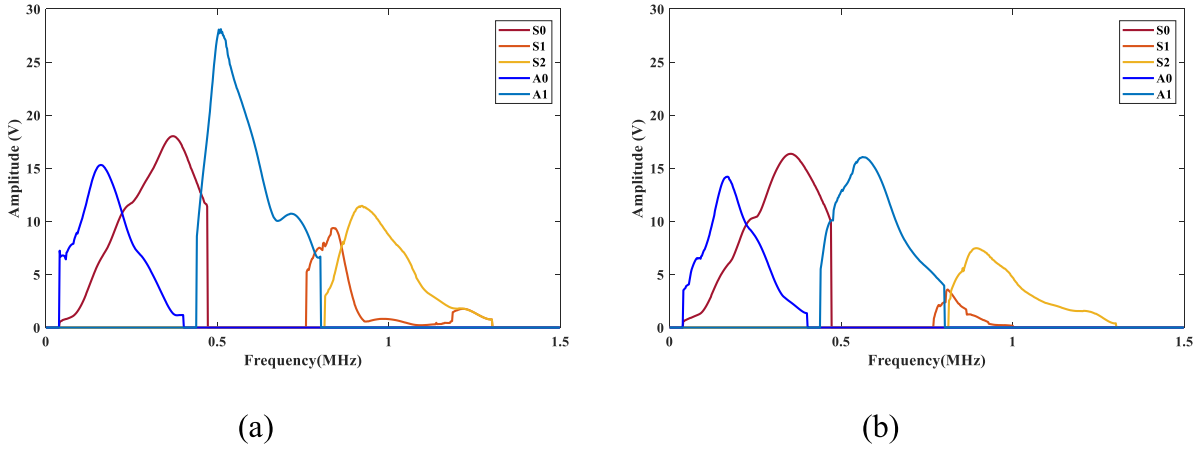

Figure 11. (a) Response amplitude of each mode from the normal path L02-P04. (b) Response amplitude of each mode from the normal path L02-P01.

Figure 9 shows the measurement arrangement. A coordinate system was employed in the monitoring area. The corrosion is at (100, 100) mm, shown as a red filled circle.

4.2. Data analysis and calculations

Sensing paths L02-P04 and L02-P01 were discussed as examples. Figure 10(a) shows the Lamb wave responses captured by the probe P04. Figure 10(c) shows the Lamb wave responses captured by the probe P01.The short-time Fourier transform (STFT) was used to map the wideband Lamb wave signal to the joint time–frequency domain. The window used is a 25 μs wide Gaussian window. Figures 10(b) and (d) show the normalized time–frequency spectrum of these two signals. The arrival dispersion curves calculated by dividing the propagation distance by the group velocity are shown in figures 10(b) and (d) (the red solid lines). It can be observed that the arrival curves matched the main energy of the individual Lamb wave mode well.

As can be seen, in the experimental signals, each mode has its own predominant frequency range. For instance, there are only A0 and S0 modes under the cutoff frequency; A1 mode is prominent in the range between the cutoff frequency of A1 and S1 (406 kHz for A1 mode and 734 kHz for S1 mode); S1 mode only exists in a narrow frequency range between the cutoff frequency of S1 and S2 (812 kHz for S2 mode); S2 mode is predominant above its own cutoff frequency. In summary, every mode would only dominate in the range between its own cutoff frequency and the cutoff frequency of the next mode.

Since different Lamb wave modes were generated in different frequency ranges, it is unnecessary to worry about the complicated mode overlap effect of multimodal Lamb waves. Therefore, single mode could be extracted from a wideband Lamb wave signal. In the time–frequency spectrum, the energy distribution of each mode can be calculated by integrating the energy in a small region near the arrival curves. Figure 11(a) shows the response amplitude of each mode of the normal path L02-P04. Figure 11(b) shows the response amplitude of each mode of the corroded path L02-P01. As can be seen, the response amplitude of the A0 and S0 modes seems have no significant difference in these two paths. While the response amplitude of A1 mode in the corroded path reduced to about half of that in the normal path. There is also a large reduction in amplitude for S1 mode and S2 mode. It can be concluded that the amplitude loss of higher-order modes can be used for corrosion detection.

4.3. Multimode-based defect detection

As shown in the results of the numerical modeling and experimental study, higher-order modes are very sensitive to corrosions while the lowest-order modes are not. Conventionally, a single higher-order mode was chosen for detecting corrosion. However, practically, detection effectiveness is highly dependent on the consistency of the sensors. That is to say,

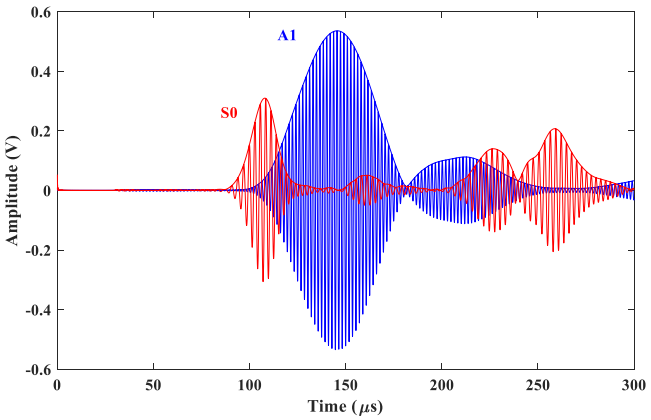

(a)

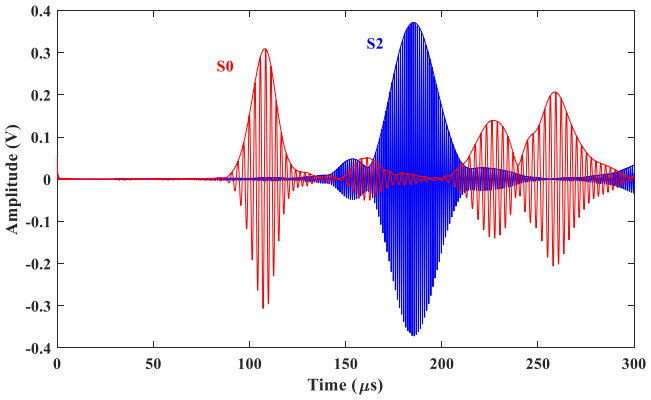

(b)

Figure 12. Narrowband extracted signals. (a) S0 mode and A1 mode. (b) S0 mode and S2 mode.

if we use a sensor array for detection, it has to be certain that the change in signals only result from defects, not from inconsistencies in the sensors. Otherwise, artificial error will be introduced. Actually, due to the difference in the manufacturing environment and the installed environment (mainly coupling conditions), the response of sensors is more or less different. Therefore, a robust method for detecting corrosions is urgently needed.

Based on the concept that each Lamb wave mode has unique sensitivity to the flaws, the multimodal Lamb wave feature can be used for corrosion detection. Rather than using narrowband excitation directly, we generated wideband Lamb waves and recorded lowest-order modes and higher-order modes simultaneously. Then a series of narrow band waveforms were extracted from the wideband signals. Afterward, we used the ratio of the amplitude of a lowest-order mode waveform and the amplitude of a higher-order mode waveform as the index for representing the corrosion, such as S0/A1 or S0/S2. Due to these two mode components from the same sensor, the ratio would remain almost the same when the Lamb wave propagates along a normal path. However, if there was any defect near the path, the index would be changed.

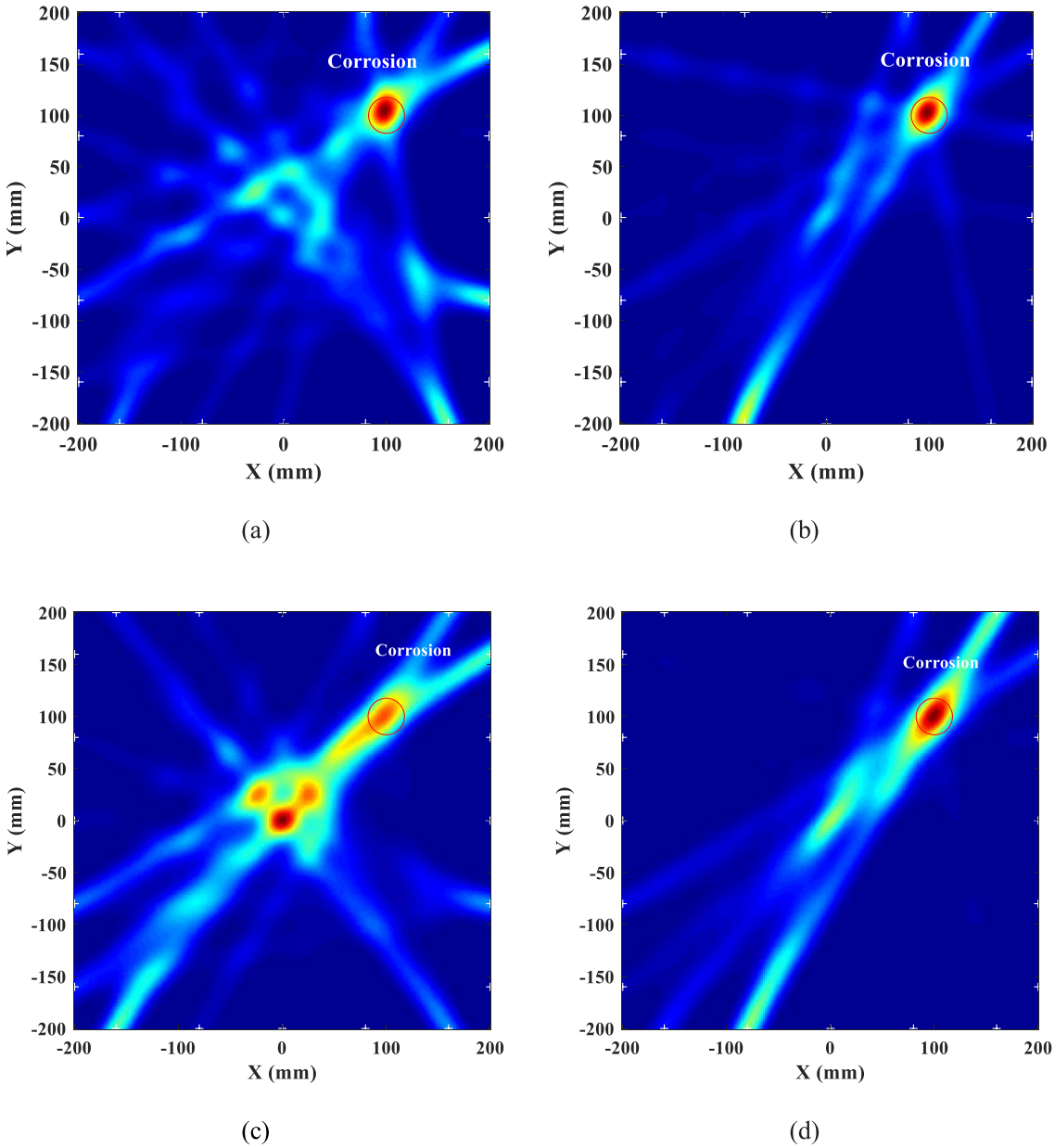

Figure 13. Location results of multimode-based defect detection method and higher-order mode defect detection. (a) S0 mode at 360 kHz and A1 mode 560 kHz. (b) S0 mode at 360 kHz and S2 mode 920 kHz. (c) A1 mode at 560 kHz. (d) S2 mode at 920 kHz.

Thus, the new index is robust regardless of inconsistency in sensors. Finally, by applying a tomographic imaging method, the corrosion can be located.

In the paper, we define the ratio of the amplitude of a lowest-order mode and a higher-order mode as the relative amplitude coefficient (*RAC*), such as $RAC_{\mathrm{S0/A1}}$ and $RAC_{\mathrm{S0/S2}}$ (equation (3)). For a normal path, *RAC* remains almost the same, but after a defect is introduced, *RAC* would increase. Usually, we chose S0 mode for the lowest-order mode, because the group velocity of S0 mode is larger than A0 mode and the dispersion effect of S0 mode is slight under the first cutoff frequency, which benefits the S0 mode extracted from a wideband signal. We would not choose S1 mode for corrosion detection, even though it showed great sensitivity to corrosions. The main reason is that S1 mode only exists in a very narrow bandwidth with a highly dispersive effect and it is hard to extract it from the overlap of A1 mode and S2 mode.

$$\begin{aligned} RAC_{\mathrm{S0/A1}} &= \frac{A_{\mathrm{S0}}}{A_{\mathrm{A1}}} \\ RAC_{\mathrm{S0/S2}} &= \frac{A_{\mathrm{S0}}}{A_{\mathrm{S2}}} \end{aligned} \tag{3}$$

where A_{S0} is the amplitude of the extracted S0 mode waveform, A_{A1} is the amplitude of the extracted A1 mode waveform, and A_{S2} is the amplitude of the extracted S2 mode waveform.

4.4. Probabilistic reconstruction algorithm

Variations in *RAC* reflect some changes resulting from structural flaws. Therefore, the probability of defect existence can be reconstructed from the severity of *RAC* change. The formula used is given as [20]

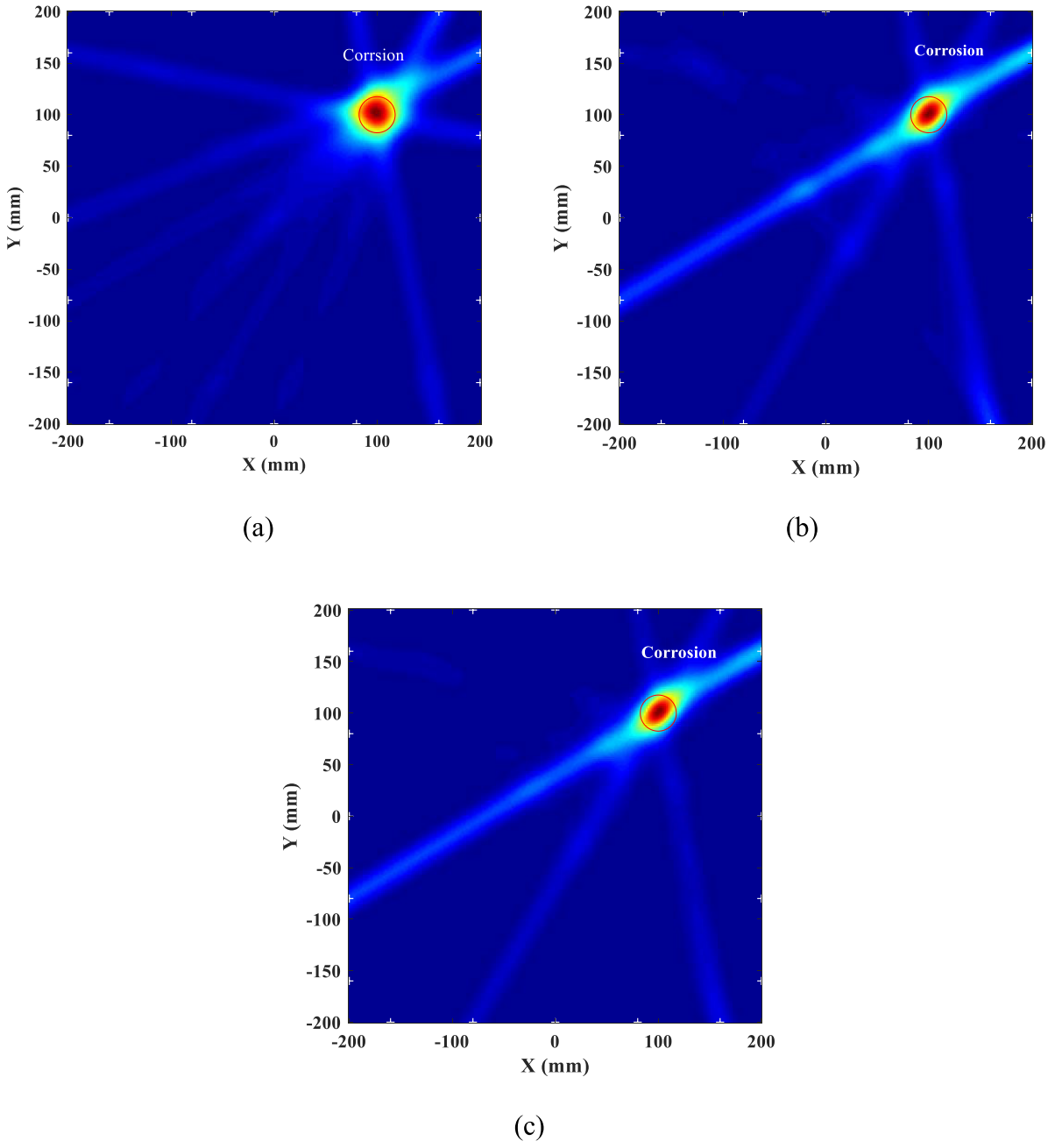

Figure 14. Location results of multimode-based defect detection method with the help of the double sensor strategy. (a) S0 mode at 360 kHz and A1 mode 560 kHz. (b) S0 mode at 360 kHz and S2 mode 920 kHz. (c) S0 mode at 360 kHz and S1 mode 800 kHz.

$$P(x,y) = \sum_{k=1}^{N} p_k(x,y) = \sum_{k=1}^{N} V_k \exp[-d_k^2/(2\sigma^2)] \quad (4)$$

where $P(x, y)$ is the defect probability estimation at position (x, y) in the reconstruction region and is a linear summation of the probability estimation from all paths. $p_k(x, y)$ is the estimation from the kth path. V_k is the variations in the *RAC* of the kth path and N is the total number of paths. V_k can be obtained by substituting RAC_k by the mean of the *RAC* of all paths. $\exp[-d_k^2/(2\sigma^2)]$ is a Gaussian function. d_k is the distance between the position (x, y) and the kth path. The Gaussian function means that the closer the defect is to the path, the larger the probability of defect occurrence. σ is the Gaussian RMS width which controls the width of the Gaussian bell and further controls the size of the effective distribution area. σ is selected to be 17.5 in this paper, which indicates the radius of the corrosion is near 17.5 mm.

$$d_k = \left| \frac{(y_{k2} - y_{k1})x - (x_{k2} - x_{k1})y + (y_{k1}x_{k2} - x_{k1}y_{k2})}{\sqrt{(y_{k2} - y_{k1})^2 + (x_{k2} - x_{k1})^2}} \right| . \quad (5)$$

4.5. Results and discussion

Considering the laser and the ultrasonic probe, acting as the transmitter and receiver, respectively, the measurement system can be considered as a linear system [21]. In a specific frequency range, the laser-generated signal can be regarded as a

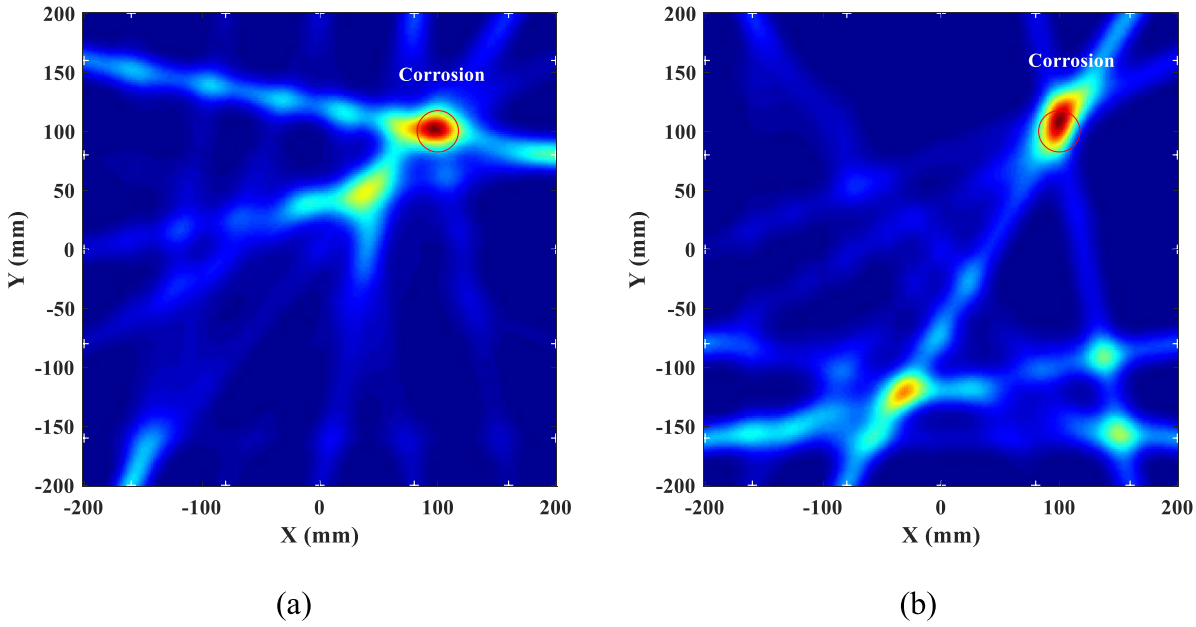

Figure 15. Location results of multimode-based defect detection method of a small corrosion. (a) S0 mode at 360 kHz and A1 mode 560 kHz. (b) S0 mode at 360 kHz and S2 mode 920 kHz.

pulse and then the received signal can be treated as pulse transfer function. The narrowband extracted signal can be obtained by convolving a desired narrowband excitation with the received signal. Figure 12(a) shows the extracted 360 kHz centered 10-cycles Hanning windowed S0 mode signal and 560 kHz centered 50-cycles Hanning windowed A1 mode signal from the normal path, L05P05. Figure 12(b) shows the extracted 360 kHz centered 10-cycles Hanning windowed S0 mode signal and 920 kHz centered 50-cycles Hanning windowed S2 mode signal. Then, by reading the peak value of the first waveform of these two signals, the ratio of amplitude of these two modes, $RAC_{S0/A1}$, $RAC_{S0/S2}$, was gained. Finally, by applying a probabilistic reconstruction algorithm, the corrosion location images can be obtained. Figures 13(a) and (b) show the location results. Both these two images show a great agreement with the real location of the corrosion. We also tried using only higher-order mode for corrosion location. The results are shown in figures 12(c) and (d). As can be seen, the multimode corrosion detection method shows better accuracy in defect location, especially for A1 mode.

The first principle of operating frequency point selection is to choose the point as close to the cutoff frequency as possible, based on the numerical study. However, the group velocity near the cutoff frequency is very small, even close to zero, which makes the mode hard to extract. The second principle is to avoid mode overlap regions, which also benefits mode extraction. In our experiment, the best operating frequency range for S0/A1 is [280, 380] kHz for S0 mode and [540, 580] kHz for A1 mode, respectively. In these frequency ranges, the location method is robust. The best operating frequency range for S0/S2 is [280, 380] kHz for S0 mode and [880, 1050] kHz for S2 mode, respectively.

Lamb wave mode overlap mainly occurred between symmetric modes and antisymmetric modes. Therefore, double sensors mounted at the top and bottom surfaces at the same position can help separate symmetric modes and antisymmetric modes by the arithmetical operations of the signals recorded by these two sensors [22]. Thus, the operating frequency range can be extended and the location accuracy be enhanced.

Figure 14 shows the location image by using the double sensor strategy. Figures 14(a) and (b) show the images of the defect location by using the same parameters as above. The location accuracy is enhanced. The effective range of A1 mode is extended to [440, 670] kHz and the range of S2 mode extended to [870, 1180] kHz. Besides, S1 mode turns out to be suitable for defect location in the frequency range [770, 830] kHz, thanks to the mode separating effect of this strategy. Figure 14(c) shows the result when we use S1 mode at 790 kHz for defect detection. In these three images, figure 14(c) is cleanest. In a word, the double sensor strategy optimizes the multimode-based defect detection method.

In order to verify the robustness of the multimodal Lamb wave corrosion detection method, an ellipsoidal corrosion of 35 mm in diameter and 0.1 mm largest depth was introduced in a normal 3.9 mm-thick aluminum plate and the double sensor strategy was also used. Figures 15(a) and (b) show the location images by using the S0/A1 mode pair and S0/S2 mode pair. As can be seen in the results, the hidden corrosion can be identified, but there are some artifacts in the image. The result shows that there is a detection limit for the proposed method and the minimum depth of corrosion which can be detected is about 0.1 mm.

5. Conclusions

In this paper, a robust corrosion detection method exploiting the multimodal Lamb wave feature is developed. Some conclusions are obtained as follows.

(i) An equal interval space sample and 2D Fourier transform can help study the interaction between Lamb wave modes and structure flaws. Based on the numerical study, thinning defects greatly decrease the transmission energy of higher-order modes, especially in the range near cutoff frequencies. Almost all the higher-order modes are sensitive to the variation in the depths of corrosions but insensitive to variation in the diameters of corrosions.

(ii) The laser and ultrasound probe can generate wideband Lamb waves. Narrowband single mode signals can be extracted by convolving desired excitations with the wideband Lamb wave.

(iii) The higher-order modes are sensitive to corrosions but the two lowest-order modes, A0 and S0, are not. Therefore, the combination of these two kinds of modes can be used to evaluate defects. The *RAC*, which is the ratio of the amplitude of the lowest-order modes and the higher-order modes, is a robust index for representing thinning defects.

(iv) Combined with a probabilistic reconstruction algorithm, the artificial corrosion can be located accurately. Either the S0/A1 or S0/S2 mode can help work out structure flaws. With the help of the double sensor strategy, the operating frequency range is extended and the location accuracy enhanced.

Acknowledgment

The work is supported by the National Natural Science Foundation of China (Grant No. 51875435, 51421004), the China Postdoctoral Science Foundation (Grant No. 2018M643627), and Beijing Key Laboratory of Measurement & Control of Mechanical and Electrical System Technology (KF20191123201) which are highly appreciated by the authors.

ORCID iDs

Zhi Luo https://orcid.org/0000-0001-9909-6900
Liang Zeng https://orcid.org/0000-0002-8945-0547
Jing Lin https://orcid.org/0000-0002-7670-1482

References

[1] Zhu W *et al* 1998 Ultrasonic guided wave NDT for hidden corrosion detection *J. Res. Nondestruct. Eval.* **10** 205–25
[2] Rose J L 2014 *Ultrasonic Guided Waves in Solid Media* (Cambridge: Cambridge University Press) (https://doi.org/10.1017/CBO9781107273610)
[3] Alleyne D and Cawley P 1991 A two-dimensional Fourier transform method for the measurement of propagating multimode signals *J. Acoust. Soc. Am.* **89** 1159–68
[4] Demma A *et al* 2003 The reflection of the fundamental torsional mode from cracks and notches in pipes *J. Acoust. Soc. Am.* **114** 611–25
[5] Tua P S, Quek S T and Wang Q 2004 Detection of cracks in plates using piezo-actuated Lamb waves *Smart Mater. Struct.* **13** 643
[6] Su Z, Ye L and Lu Y 2006 Guided Lamb waves for identification of damage in composite structures: a review *J. Sound Vib.* **295** 753–80
[7] McKeon J C P and Hinders M K 1999 Parallel projection and crosshole Lamb wave contact scanning tomography *J. Acoust. Soc. Am.* **106** 2568–77
[8] Kundu T, Potel C and De Belleval J F 2001 Importance of the near Lamb mode imaging of multilayered composite plates *Ultrasonics* **39** 283–90
[9] Alleyne D N and Cawley P 1992 The interaction of Lamb waves with defects *IEEE Trans. Ultrason. Ferroelectr. Freq. Control* **39** 381–97
[10] Lee B C and Staszewski W J 2003 Modelling of Lamb waves for damage detection in metallic structures: part II. Wave interactions with damage *Smart Mater. Struct.* **12** 815
[11] Leonard K R, Malyarenko E V and Hinders M K 2002 Ultrasonic Lamb wave tomography *Inverse Problems* **18** 1795
[12] Zhao M *et al* 2014 Mode identification and extraction of broadband ultrasonic guided waves *Meas. Sci. Technol.* **25** 115005
[13] Li F *et al* 2009 Dispersion analysis of Lamb waves and damage detection for aluminum structures using ridge in the time-scale domain *Meas. Sci. Technol.* **20** 095704
[14] Meguid S A and Wang X D 1999 Wave scattering from cracks and imperfectly bonded inhomogeneities in advanced materials *Mech. Mater.* **31** 187–95
[15] Al-Nassar Y N, Datta S K and Shah A H 1991 Scattering of Lamb waves by a normal rectangular strip weldment *Ultrasonics* **29** 125–32
[16] Chang Z and Mal A 1999 Scattering of Lamb waves from a rivet hole with edge cracks *Mech. Mater.* **31** 197–204
[17] Zhu W, Rose J L and Agarwala V S 1999 Experimental study on hidden corrosion/delamination detection with ultrasonic guided waves *Review of Progress in Quantitative Nondestructive Evaluation* vol 18 A eds D O Thompson, D E Chimenti (Boston, MA: Springer) (https://doi.org/10.1007/978-1-4615-4791-4_231)
[18] Silva M Z, Gouyon R and Lepoutre F 2003 Hidden corrosion detection in aircraft aluminum structures using laser ultrasonics and wavelet transform signal analysis *Ultrasonics* **41** 301–5
[19] Zeng L *et al* 2017 Excitation of Lamb waves over a large frequency-thickness product range for corrosion detection *Smart Mater. Struct.* **26** 095012
[20] Zhao X *et al* 2011 Ultrasonic Lamb wave tomography in structural health monitoring *Smart Mater. Struct.* **20** 105002
[21] Michaels J E *et al* 2013 Chirp excitation of ultrasonic guided waves *Ultrasonics* **53** 265–70
[22] Su Z and Ye L 2004 Selective generation of Lamb wave modes and their propagation characteristics in defective composite laminates *Proc. Inst. Mech. Eng.* L **218** 95–110